Synthesis and characterization of Sr-doped NaTaO[3] photocatalysts for water splitting

An, Longjie

(Degree)
博士（理学）

(Date of Degree)
2017-09-25

(Date of Publication)
2018-09-01

(Resource Type)
doctoral thesis

(Report Number)
甲第6997号

(URL)
https://hdl.handle.net/20.500.14094/D1006997

(別紙様式 3)

論 文 内 容 の 要 旨

氏　名：　安 龍杰

専　攻：　化学専攻

論文題目（外国語の場合は，その和訳を併記すること。）

Synthesis and characterization of
Sr-doped $NaTaO_3$ photocatalysts for water splitting

和訳：　Sr ドープ $NaTaO_3$ 水分解光触媒の合成と特性分析

指導教員：　大西 洋

Synthesis and characterization of Sr-doped $NaTaO_3$ photocatalysts for water splitting

1. Introduction

Energy is an essential element to our lives as well as food in the 21st century. Due to high energy dependence, energy demand increased significantly. To solve the energy resource defect the human society may face in future, sustainable energy technologies are under development. In this thesis, the author focused on the study of water splitting photocatalyst.

Sunlight power can be converted to chemical energy to split water into H_2 and O_2 through photocatalysis reaction. Hydrogen product is a clean energy source that can be converted to electricity via fuel cells. The water splitting reaction process can be divided into three steps. As the first step, electron-hole incident light excites the electrons at valence band to conduction band, leaving holes at valence band. As the second step, some of excited electrons will recombine soon with holes due to the energy difference, and the others being alive. As the final step, the alive carriers will move to the surface of photocatalyst particles where the water splitting reaction occurs. In the second step, the restriction to electron-hole recombination plays a key role to increasing efficiency.

In the previous study, metal dopants restricted efficiently the electron-hole recombination, such in metal-doped $NaTaO_3$. The La-doped $NaTaO_3$ exhibited the highest quantum efficiency of water splitting at 56% under UV irradiation with 270 nm. Doping of alkaline earth metals (Sr, Ba) showed comparable efficiency as La doping. Increased efficiency induced by metal doping is attributed to restricted electron-hole recombination. In this thesis, Sr-doped $NaTaO_3$ was mainly studied to understand deeply on the effect of the metal dopants on $NaTaO_3$ photocatalyst.

2. Experimental section

In the solid-state method (SSM), mixtures of Na_2CO_3, Ta_2O_5, and $SrCO_3$ were calcined in an alumina crucible at 1173 K for 1 h and then at 1423 K for 10 h to produce Sr-doped $NaTaO_3$ (Sr-NTO). In the hydrothermal method (HTM), 4 mol L^{-1} aqueous solution of NaOH containing Ta_2O_5, and $SrCO_3$ were stirred and sealed in a Teflon container. The mixture was

heated at 433 K for 24 h in an autoclave. In the molten salt method (MSM), mixtures of Na_2CO_3, Ta_2O_5, $SrCO_3$, and NaCl (flux) were calcined in an alumina crucible at 1423 K for 1-60 h. In the HF etching, as prepared Sr-NTO was stirred in Teflon jar containing an aqueous HF solution (10 wt%, 3 ml) for 10 mins and then washed with purified water until to get a neutral fluid.

Elemental composition in bulk and on surface was measured by energy dispersive X-ray spectroscopy (EDX) and X-ray photoelectron spectroscopy (XPS). The crystallographic phase was determined by X-ray diffraction (XRD). Raman scattering was detected by Raman spectroscopy. Band gap energy was obtained by UV-Vis diffuse-reflection spectroscopy. Particle shape and size were observed by scanning electron microscopy (SEM). The local structure of Sr was detected by X-ray absorption spectroscopy (XAS). The steady-state population of UV-excited electrons not yet recombined with holes was measured by infrared (IR) absorption spectroscopy upon UV light irradiation. The radial distribution of Sr was examined by scanning transmission electron microscopy (STEM) lined with EDX.

3. Results and discussion

Figure 1 shows XRD (110) peaks, referring to a single phase of perovskite-structured $NaTaO_3$, of Sr-NTOs (SSM). The gradual low-angle shifts caused by increasing Sr concentration indicate perovskite lattice expansion. The ionic radii of 6-fold-coordinated Ta^{5+} (B-site) and Sr^{2+} are 0.06 and 0.12 nm, respectively. Meanwhile, the ionic radii of 12-fold-coordinated Na^+ (A-site) and Sr^{2+} are both 0.14 nm. Therefore, the lattice expansion should be contributed mainly from B-site doping of Sr. Here the Sr-doped $NaTaO_3$ with input Sr concentration at 200 mol% produced $Sr(Sr_{1/3}Ta_{2/3})O_3$, which has a perovskite structure with parts of B-sites substituted by Sr. The lattice volume increased consistently with Sr concentration in a range of 0-200 mol%. It suggests solid solutions between $NaTaO_3$ and $Sr(Sr_{1/3}Ta_{2/3})O_3$. As one idea, the $Sr(Sr_{1/3}Ta_{2/3})O_3$ can be explained as all the A-sites and parts of B-sites of $NaTaO_3$ were replace with Sr. Hence the Sr should substitute both A- and B-sites when doped via SSM.

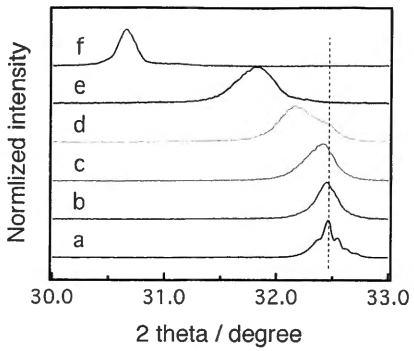

Figure 1. XRD (110) peaks of Sr-NTO with input Sr concentration at (a) 0 mol%, (b) 2 mol%, (c) 8 mol%, (d) 20 mol%, (e) 50 mol%, and (f) 200 mol%.

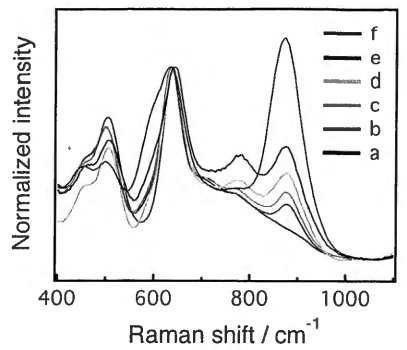

Figure 2. Raman spectra of Sr-NTO with input Sr concentration at (a) 0 mol%, (b) 1 mol%, (c) 2 mol%, (d) 5 mol%, (e) 8 mol%, and (f) 20 mol%.

The B-site doping was supported by detection on Raman scattering, as shown in **Fig. 2**. In addition to major Raman bands appeared at 450, 500, and 620 cm^{-1} referring to pristine NTO, Sr doping produced two Raman bands at 860 and 760 cm^{-1}. These bands are assigned to breathing vibrations of BO_6 octahedra in B-site substituted perovskite, $A(B_{1-x}B'_x)O_3$. The BO_6 breathing mode (A_{1g} symmetry) will produce Raman bands in a range of 750-900 cm^{-1} when symmetry restriction in an ideal perovskite ABO_3 was broken by partial substitution of B-site cations with hetero-cations (B'). The additional Raman bands observed at 860 and 760 cm^{-1}, thus, indicate at least partial Sr substituted B-sites of NTO when doped via SSM.

To support the simultaneous A- and B-site doping of Sr in Sr-NTO (SSM), the local structure of Sr was observed by XAS. In the interpretation of extended X-ray absorption fine structure (EXAFS), two different Sr-O coordinations were detected. Results of curve fitting on each Sr-O coordination explain the two coordination are assigned to Sr(B)-O and Sr(A)-O, respectively, where Sr(B) or Sr(A) means the Sr doped at B- or A-sites. In SSM, Sr substituted both A- and B-sites to form a $NaTaO_3$-$Sr(Sr_{1/3}Ta_{2/3})O_3$ solid solution.

The combination of EDX and XPS suggest a high Sr segregation on the particle surface of Sr-NTO (SSM). The Sr doping produced a core-shell structure with a Sr-pool core covered by a Sr-rich shell. The core-shell structured $NaTaO_3$-$Sr(Sr_{1/3}Ta_{2/3})O_3$ solid solution affected strongly by the particle size and shape. **Figure 3** shows SEM images of Sr-NTOs (SSM).

Doping of Sr at 0.1 and 0.3 mol% reduced the particle size of NTO from 5 μm to 500 nm or smaller. Sr with larger concentration at 0.5-2.0 mol% induced surface reconstruction. The steps and terraces were produced on particle surface to release lattice mismatch at the epitaxial interface between the Sr-poor core and Sr-rich shell. The picture of core-shell structured $NaTaO_3$-$Sr(Sr_{1/3}Ta_{2/3})O_3$ solid solution provided a simple explanation of the surface reconstruction induced by Sr doping via SSM.

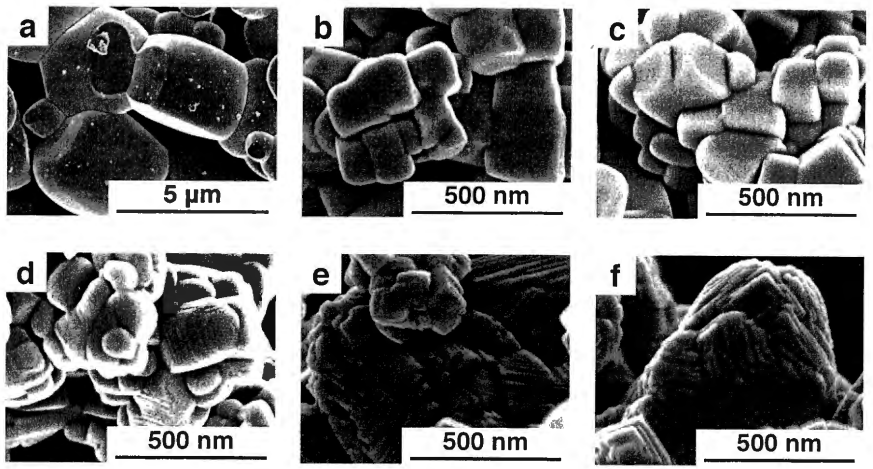

Figure 3. SEM images of Sr-NTO with input Sr concentration at (a) 0 mol%, (b) 0.1 mol%, (c) 0.3 mol%, (d) 0.5 mol%, (e) 1 mol%, and (f) 2 mol%.

On the other hand, in Sr-NTO prepared via HTM, the lattice expansion and the additional Raman bands were absent. Consequently, the particle surface was not reconstructed to steps and terraces. All the results suggest a single A-site doping of Sr in HTM.

The effect of B-site doped Sr on the electron-hole recombination was detected by UV-induced IR absorption spectroscopy. **Figure 4** shows the change in IR absorbance before and after UV irradiation of NTO and Sr-NTO (2 and 8 mol%) prepared via SSM and HTM. The IR absorbance change, which increased monotonically from 6000 to 900 cm^{-1}, presents the population of band gap excited electrons that not yet recombined with holes. In HTM, the population of excited electrons barely changed before and after Sr doping. On the contrary, the electron population increased drastically with Sr doping via SSM. The integrated

absorbance in a range of 6000-900 cm^{-1} was enhanced by 180 times in Sr-NTO (SSM) relative to that of NTO (SSM). The contrasting results in SSM and HTM show the Sr doped at B-sites should play a key role to restriction of the electron-hole recombination.

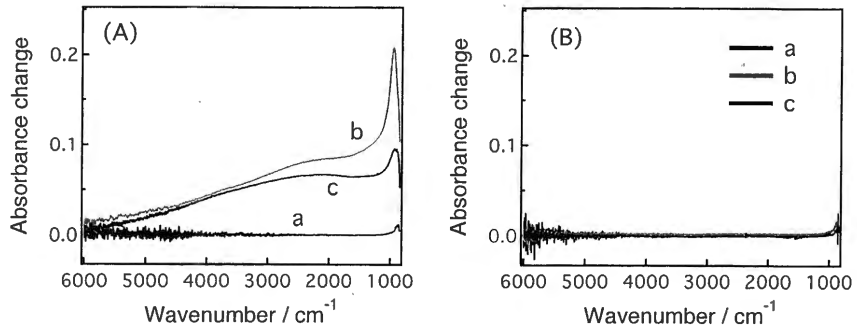

Figure 4. Change in IR absorbance induced by UV light irradiation of Sr-NTO with input Sr concentration at (a) 0 mol%, (b) 2 mol%, (c) 8 mol%. Sr-NTOs were prepared via (A) SSM and (B) HTM.

In SSM, the population of excited electrons increased to a maximum with Sr concentration at 2 mol% but then decreased gradually with Sr concentration larger than 2 mol%. The sudden reduction in the electron population should be affected by another factor rather than the Sr doped at B-sites. 5 mol% Sr-NTO (SSM) was chemically etched with HF solution to examine the effect of the radial distribution of Sr on the electron-hole recombination.

The change in particle size and shape during HF etching on the Sr-NTO was observed by SEM. As the HF etching increased from 10 to 480 m, the particle size of Sr-NTO decreased consistently.

The Sr concentrations in bulk and on surface before and after etching were detected by EDX and XPS, respectively. The bulk Sr concentration decreased rapidly from 5.1 mol% to 4.6 mol% during etching till 10 m and then decreased gradually to 3.4 mol% during etching within 480 m. The reduction of the surface Sr concentration by etching presented two-step response as well as in bulk. Surface Sr concentration decreased rapidly from 19.9 mol% to 17.0 mol% in 10 m-etching, and then gradually decreased to 12.4 mol% in 480 m-etching. The two different period of response on the Sr reduction both in bulk and on surface supports the core-shell structure with a Sr-poor core covered by a Sr-rich shell. The rapid reduction of

Sr concentration by etching in 10 m indicates the shell possesses a serious Sr segregation. And the gradual decrease of Sr concentration by etching in 10-480 m suggests a Sr concentration gradient in the core.

Compared to the EDX and XPS quantifying the total concentration of Sr doped at A- and B-sites, the Raman spectroscopy was able to detect concentration change in the Sr doped at B-sites alone. In SSM, the Sr doping produced Raman band with clear intensity at 860 cm^{-1}. The band intensity increased consistently with Sr concentration. Therefore, it can be used to trace Sr concentration change during etching. **Figure 5** shows the intensity ratio of 860/620 cm^{-1} band plotted as a function of etching time. The relative intensity of 860 cm^{-1}-band was reduced about 30 % for 10m-etching, followed by a gradual reduction for longer etching. This two-step response by HF etching on the decrease of 860 cm^{-1} band intensity indicates similar results as EDX and XPS, that is the shell has a serious concentration of Sr doped at B-sites, and the core has a concentration gradient of Sr doped at B-sites (CGSrB). Meanwhile, the 760 cm^{-1} band was removed fully for 10m-etching. It means the Sr segregation on the shell produced the unexpected component.

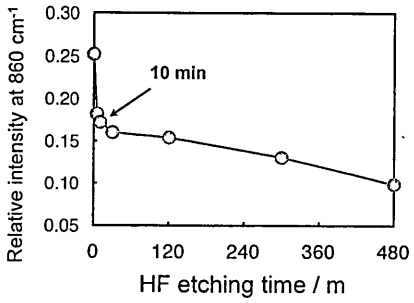

Figure 5. Relative intensity of Raman band at 860 cm^{-1} to 620 cm^{-1} in 5mol% Sr-NTO (SSM) as a function of etching time in a range of 0-480 m.

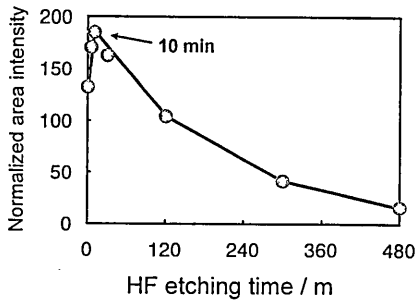

Figure 6. Integrated IR absorbance change upon UV irradiation of 5mol% Sr-NTO (SSM) relative to that of NTO (SSM) as a function of etching time in a range of 0-480 m.

The change in the population of excited electrons during etching was examined by UV-induced IR absorption spectroscopy. For a direct visualization of the change in electron population during etching, the IR absorbance change was integrated into a range of 6000-900 cm^{-1}. **Figure 6** shows a plot of the integrated absorbance change of etched 5 mol% Sr-NTO relative to that of pristine NTO as a function of etching time. Here the integration intensity is proportional to the population of UV-excited electrons. The electron population of unetched Sr-NTO was 132 times as much as NTO. During etching on the shell for 10 m, the relative electron population of Sr-NTO increased by 40% to 185 times. On the other hand, longer etching mainly on the core reduced the electron population gradually, eventually, reaching to 16 times for 480 m-etching. It indicates the electrons and holes were excited in the core but recombined in the shell.

According to Raman scattering, two components showing 760 and 860 cm^{-1} Raman bands were detected in the shell. The unexpected component might accelerate the electron-hole recombination. More important issue is the restricted electron-hole recombination in the core. The author proposes that the CGSrB restricted the recombination.

In the detection of band gap energy in Sr-NTO (SSM) by UV-Vis spectroscopy, the central wavelength of the absorption edge was gradually shifted to shorter wavelength upon doping of Sr. It shifted from 305 nm in pristine NTO to 280 nm in 50 mol% Sr-NTO. It indicates the expansion of band gap energy. The condition band (CB) of NTO is mainly derived from Ta 5d orbitals while the valence band (VB) is derived from O 2p orbitals. Sr doping should contribute little to the VB potential but affect the CB. The expansion of band gap energy can be explained by the upward shift of CB minimum potential due to the connections of the Ta 5d orbitals were cut the Sr doping at B-sites. Based on this assumption, the CGSrB in the core will produce a potential gradient of CB minimum with more negative potential in the outer core than in the inner core, as shown in **Fig. 7**. The steady-state UV-excited electrons were driven through the CB potential gradient from outer core to inner core for separating from the holes leaving in the outer core. In this picture, the electron-hole recombination is restricted by CGSrB.

In the following step, the role of CGSrB to electron-hole recombination was intensely studied by strategical synthesis of 2 mol% Sr-NTOs with various CGSrB degree. To control the radial distribution of Sr, MSM was applied to prepare Sr-NTOs by adjusting heating time.

Four Sr-NTOs were synthesized via MSM with heating time at 1 h, 10 h, 20 h, and 60 h, respectively, in addition to undoped NTO heated for 10 h. The Sr concentration of each Sr-NTO was 2.0 mol% when examined by EDX. Particle size and shape were similar in the four

Sr-NTOs, as observed by SEM. All the samples produced the Raman band at 860 cm^{-1}. The band intensity was reduced gradually with increased heating time at 1-60 h. However, the reduction was limited to provide a strong evidence that the four Sr-NTOs were prepared differently.

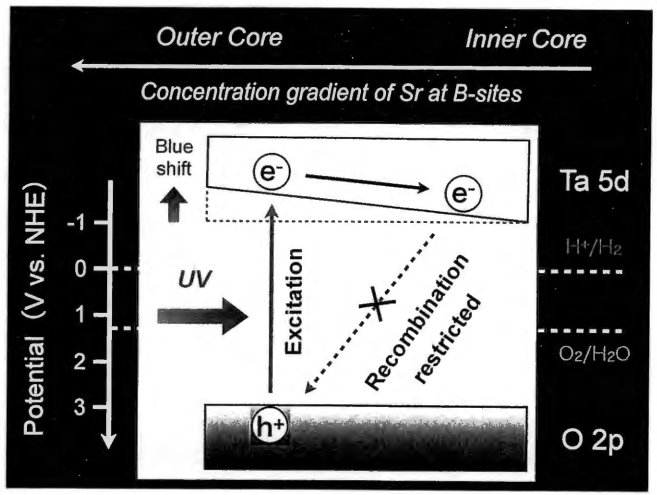

Figure 7. Mechanism of electron-hole separation driven by potential energy gradient of conduction band.

Although the particle size and shape, the Sr concentration in total and at B-sites were similar in the four Sr-NTOs prepared by distinct heating time, the electron-hole recombination rate was very different. **Figure 8** shows a plot of the integrated IR absorbance change (6000-900 cm^{-1}) of each Sr-NTO normalized to that of NTO. The relative electron population decreased consistently from 159 to 9 with extended heating time in 1-60 h. The drastic change in electron population by heating time was attributed to the distinct degree of CGSrB in the four Sr-NTOs.

The radial distribution of Sr in the two typical Sr-NTOs, heated for 1 or 60 h, was examined by STEM lined with EDX. As a result, Sr segregated on the surface of a Sr-NTO particle heated for 1 h, in contrast to a homogeneous distribution of Sr in a 60h-heated Sr-NTO

particle. It supports the significant role of CGSrB to the efficient restriction of electron-hole recombination.

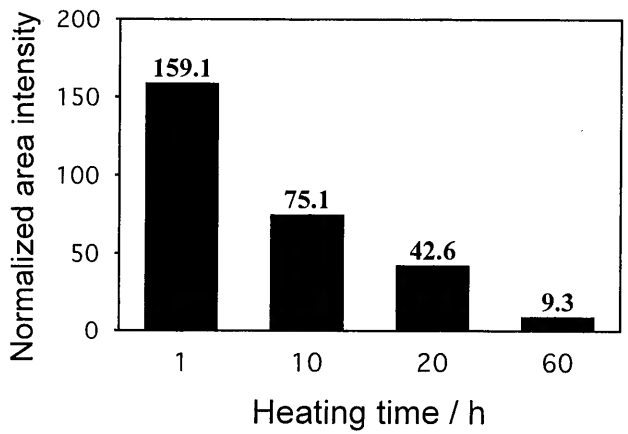

Figure 8. Integrated IR absorbance change induced by UV irradiation of Sr-NTOs (MSM) relative to that of NTO (MSM) as a function of heating time.

（別紙１）　　論文審査の結果の要旨

氏名	安　龍杰		
論文題目	Synthesis and characterization of Sr-doped $NaTaO_3$ photocatalysts for water splitting （Sr ドープ $NaTaO_3$ 水分解光触媒の合成と特性分析）		
審査委員	区　分	職　名	氏　　名
	主　査	教授	大西　洋
	副　査	教授	小堀康博
	副　査	准教授	高橋一志
	副　査	特命准教授	笹原　亮
	副　査		

要　　旨

申請者（安龍杰氏）が提出した学位論文を、本研究科の学位論文評価基準に照らして審査するために、物理化学講座教員３名（大西・小堀・笹原）と無機化学講座教員１名（高橋）からなる審査委員会を組織した。平成 29 年 8 月 11 日 10 時 40 分から審査委員全員の出席のもとで、安氏による学位論文発表会を開催して発表 40 分に続き 50 分にわたって論文内容と関係学術分野に関する口頭試問をおこなった。試問終了後ただちに審査委員会を開催して、学位論文評価基準が定める以下の５項目について各委員の心証を意見交換したのちに合否を判定した。

（1）専攻分野に関する高度な学術的価値を有する研究結果を含むこと

光触媒による人工光合成の量子収率を上げるためにはバンドギャップ励起によって生じる電子と正孔の再結合を抑制しなければならない。ランタノイドまたはアルカリ土類金属を数 mol%ドーピングすることで $NaTaO_3$ 光触媒の電子-正孔再結合が抑制されて、非常に高い（50%超）量子効率で水を全分解することが先行研究で明らかとなっている。

金属ドーピングが再結合を抑制するメカニズムを明らかにすることを目的とした本研究は、Sr^{2+} をドーピングした $NaTaO_3$ に焦点を絞って、①ドーピングした Sr^{2+} が Ta^{5+} を置換してペロブスカイト型結晶格子の B サイトを占有すること、および②B サイトを占有する Sr^{2+} が 0.1 μm サイズの $NaTaO_3$ 微粒子内で動径方向に濃度傾斜をもつことが、再結合抑制に必要であることを実験的に示した。これらの成果は（$NaTaO_3$ に限らず）より活性の高い光触媒を開発する知的基盤として疑いなく重要である。イオン半径の類似性から Na^+（A サイト）を置換すると信じられてきた Sr^{2+} が、Ta^{5+}（B サイト）を置換することを発見し、高効率光触媒材料を研究することで未知のサイエンスを発見できることを示した意義は大きい。とくに、申請者は金属ドーピングが伝導体下端のエネルギー傾斜を作って電子-正孔再結合を抑制することを提案した。本提案はこれから広く検証されるべき重要な意味をもつ。

（2）先行研究や関連研究をふまえて適切な課題設定をおこなっていること

人工光合成の実現をめざしてこれまで探索されてきた膨大な光触媒材料のなかから、世界最高の量子効率で水を完全分解する $NaTaO_3$ に着目し、異種金属ドーピングによる効率向上のメカニズム解明に的を絞った課題設定は時宜を得た適切なものである。

氏名	安　龍杰

（3）課題に対して適切な研究方法を選択し研究を実施していること

$NaTaO_3$ にドーピングした Sr^{2+} が、ペロブスカイト型結晶格子の A サイトまたは B サイトのどちらを占有するかを推定するためにラマン分光の選択律を利用し、推定構造をエックス線吸収分光による構造決定で確認した実験手法は適切である。溶融塩合成法での加熱時間を 1 から 60 時間まで延長すると $NaTaO_3$ 微粒子内の Sr^{2+} 分布が平均化することを利用して、Sr^{2+} の濃度勾配が再結合抑制を支配する要因であることを見いだした研究計画は適切である。

（4）研究結果を適切に考察し結論を得ていること

研究当初に Sr^{2+} をドーピングした $NaTaO_3$ 光触媒を固相合成と水熱合成によって調製し、両者がまったく異なるラマンスペクトルを与えることを偶然発見したことを看過せずペロブスカイト型結晶のラマン選択律をもとに禁制/非禁制を考察して Sr^{2+} の B サイト置換を提案した。さらに化学エッチングによる再結合速度の変化をもとに Sr^{2+} 濃度勾配の重要性を発想し、これを実証するために溶融塩合成法による光触媒調製までを実施した研究デザインは適切であり、安氏が従来説にとらわれない柔軟な発想をもとに研究を展開する能力をもつことを示している。Sr^{2+} ドーピングが電子-正孔再結合を抑制するメカニズムとして Sr^{2+} 濃度傾斜がつくりだす伝導帯下端のエネルギー傾斜を提案したことも適切である。当該提案の成否は今後の電子状態シミュレーションなどの結果を待つとしても、現時点で収集した実験事実にもとづく考察としては蓋然性が高い。

（5）章立て・引用を含めて論理的で明瞭な記述をおこなっていること

研究の背景と目的（1 章）・光触媒合成と計測評価手法の原理（2 章）・合成方法によるドーピングサイトの変化（3 章）・化学エッチングによる再結合速度の変化（4 章）・合成中の加熱時間による再結合速度の変化（5 章）・エックス線吸収スペクトルによる Sr^{2+} の局所構造決定（6 章）・総括（7 章）からなる学位論文の章立ては適切である。各章ともに目的・実験手順・実験結果が、申請者の考察と区別して記述されており、学位論文として十分に論理的かつ明瞭に記されている。人工光合成の実現をめざす膨大な先行研究のなかで、自らの研究に関係する論文を適切に引用している。

【結論】以上の認識にもとづいて本審査委員会は、安氏が提出した学位論文が学位論文評価基準をみたし、人工光合成をめざす光触媒の基礎研究を進展させた成果として学位授与にふさわしい内容をもつと全員一致で判定した。